行政院國家科學委員會補助專題研究計畫 ■ 成 果 報 告 □期中進度報告

以衛星測高及重力決定台灣東部黑潮之流場及其時變(3/3)
Determination of velocity field of kuroshio east of Taiwan and its temporal variation using satellite altimetry and gravity data(3/3)

計畫類別：■ 個別型計畫　□ 整合型計畫
計畫編號：NSC　96－2611－ M －009－001－
執行期間：　96　年　8 月　1　日至　97　年　7 月 31 日

計畫主持人：黃金維
共同主持人：
計畫參與人員： 施亘昶、蕭宇伸、曾子榜

成果報告類型(依經費核定清單規定繳交)：□精簡報告　■完整報告

本成果報告包括以下應繳交之附件：
□赴國外出差或研習心得報告一份
□赴大陸地區出差或研習心得報告一份
□出席國際學術會議心得報告及發表之論文各一份
□國際合作研究計畫國外研究報告書一份

處理方式：除產學合作研究計畫、提升產業技術及人才培育研究計畫、列管計畫及下列情形者外，得立即公開查詢
□涉及專利或其他智慧財產權，□一年□二年後可公開查詢

執行單位：國立交通大學

中　華　民　國　　97 年　　10 月　　31 日

行政院國家科學委員會專題研究計畫成果報告

以衛星測高及重力決定台灣東部黑潮之流場及其時變(3/3)

Determination of velocity field of kuroshio east of Taiwan and its temporal variation using satellite altimetry and gravity data(3/3)

計畫編號：NSC 96－2611－M－009－001

執行期限：96 年 8 月 1 日至 97 年 7 月 31 日

主持人：黃金維　　國立交通大學土木工程學系

計畫參與人員：施亘昶　　國立交通大學土木工程學系

蕭宇伸、曾子榜　國立交通大學土木工程學系

1. Introduction

Tools for observing ocean currents can be surface and space-based. One of the space-based tools is satellite altimetry. A comprehensive document of techniques and applications of satellite altimetry can be found in Fu and Cazenave (2001). Oceanographic studies around Taiwan based on altimetry are abundant in the literature. The most frequently investigated subjects, among others, are the Kuroshio and eddies east of Taiwan, tides, circulations and eddies in the South China Sea, and tides in the Taiwan Strait. Due to shallow waters and bad altimetry data quality, ocean currents in the Taiwan Strait solely derived from altimetry are, however, not seen in the literature. In this project, we employed specially designed filter and waveform retracking to improve the quality of the altimeter data over shallow waters around Taiwan.

Varying at different spatial and temporal scales, ocean currents around Taiwan are rather diversified (Liang et al., 2003). Originating in the tropical Pacific, the Kuroshio lies east of Taiwan and is one of the major western boundary currents in the world ocean. The South China Sea is situated south of Taiwan and is a semi-closed sea, and here the circulations are largely affected by monsoonal winds and are therefore mostly seasonal. Both the Kuroshio area and the South China Sea are abundant with warm and cold-cored eddies (Hwang et al., 2004). The Taiwan Strait lies west of Taiwan and is a newly explored area in terms of oceanography and here numerous findings in the 2000s have filled the information gaps; see, e.g., Chen and Shen (2006). North of Taiwan lies the East China Sea, where the Kuroshio “intrudes” into the continental shelf in the winter time (Tang et al., 2000). These four oceanic zones are now under intensive studies in the world oceanographic community.

This project does not attempt to study all these ocean currents by satellite altimetry. Rather, we will investigate an altimetry-based method that can determine time-varying geostrophic ocean current components. We choose to use TOPEX/Poseidon (T/P) and JASON-1 altimeter data. These two missions are specifically designed for oceanographic applications. The 10-day repeat period is ideal for seeing short-term variations of oceanic signals. Our method requires an accurate geoid model and accurate sea surface heights (SSHs) from altimetry. Also, 2-dimensional mean ocean current field over the Kuroshio Current east of Taiwan will be derived from satellite altimeter data and a geoid model.

2. Improving satellite altimeter data: filtering, despiking and filtering

2.1 Despiking and filtering

Outliers in altimeter data will create a damaging effect on the resulting gravity fields and must be removed before filtering. We use an iterative method to detect outliers in along-track altimeter data. Consider a time series of along-track altimeter observable with the along-track distance as the independent variable. First, a filtered time series is obtained by convolving the original time series with the Gaussian function

$$f(x) = e^{-\frac{x^2}{2\sigma^2}} \qquad (1)$$

where x is the distance between two data points and σ is the 1/6 of the given filter width of convolution. A filter width is the size of a window within which all data points are convolved with the Gaussian function. The definition of the Gaussian function in (1) is the same as that defined in module "filter1d" of GMT (Wessel and Smith, 1995). For all data points the differences between the original and the filtered values are computed, and the standard deviation of such differences is determined. The largest difference that also exceeds three times of the standard deviation is considered an outlier and the corresponding data value is removed from the time series. The initially cleaned time series is filtered again and the new differences are examined against the new standard deviation to remove remaining outliers. This process is repeated and terminated when no outlier is found. It turns out differenced height is more sensitive to outlier than SSH, especially when along-track SSHs experience an abrupt change. A spike of SSH will create two distinct height differences. We experimented with several filter widths. It is concluded that different filter widths should be used for different sets of altimeter data for a best result. Based on testing results, we adopt 28 km and 18 km as the optimal filter widths for the repeat and non-repeat missions, respectively. More detail on the outlier detection can be found in Hwang and Hsu (2008).

2.2 Altimeter waveform retracking

Waveforms are a series of powers at altimeter gates generated by a returning pulse of altimeter from the sea. In the open ocean, waveforms are assumed to follow the ocean functional of Brown (1977) and the corresponding range between the antenna and the sea is derived from an onboard tracker based on such waveforms. There are numerous methods for waveform retracking. In this project, we experimented with four methods that are both based on functional fit and statistics. For the method of functional fit, we chose to use the Beta-5 retracker (Martin et al., 1983; Anzenhofer and Shum, 2002), which fits waveforms by the function

$$y_t = \beta_1 + \beta_2(1+\beta_5 Q)p\left(\frac{t-\beta_3}{\beta_4}\right) \qquad (2)$$

with

$$Q = \begin{cases} 0 & for \quad t < \beta_3 + 0.5\beta_4 \\ t - (\beta_3 + 0.5\beta_4) & for \quad t \geq \beta_3 + 0.5\beta_4 \end{cases} \qquad (3)$$

$$p(x) = \frac{1}{\sqrt{2\pi}} \int_{-\infty}^{x} \exp\left(\frac{-q^2}{2}\right) dq \qquad (4)$$

where y_t is the power at gate t (t ranges from 1 to 60 for Geosat), β_1 is thermal noise, β_2 is the amplitude, β_3 is the gate at the center of the leading edge, β_4 is the half ascending time of the leading edge, and β_5 is the slope of the trailing edge.

In the case of complex waveforms, the threshold retracker cannot properly determine the center of the leading edge. In this project we developed an improved threshold retracker. First, the difference between the powers of every other two gates is computed. If half of the difference is greater than a given value ε_1, then it shows that the antenna begins to pick up the returning power. In this case (difference $> \varepsilon_1$), the difference between two successive powers is then computed. If this difference is greater than a given value ε_2, then it indicates that the antenna continues to pick up the returning power, and the corresponding gate and power are included in the first sub-waveform. The selection of sub-waveform gates is terminated when the difference is smaller than ε_2. Both ε_1 and ε_2 are determined empirically, and it is found that the result with $\varepsilon_1 = 8$, and $\varepsilon_2 = 2$ is the best. The sub-waveform is then extended by including four gates at the beginning and the end of the sub-waveform. Using the selected samples in the sub-waveform, a retracking gate corresponding to this sub-waveform is determined. At the final step, we compare the previous SSH with the current SSHs associated with the computed retracking gates to make decision: the "best" retracking gate is the one that yields the smallest difference between the current SSH and the previous SSH. Table 1 compares the performances of different retrackers. Clearly the improved threshold method delivers the best result. More detail of this method is given in Hwang et al. (2006), Chang et al. (2005) and Guo et al. (2006).

Table 1: Statistics of waveform retracking for Geosat/GM track 85206

Retracker	Total No.	Processed No.	Ratio	Std dev of difference[1] (m)
Beta-5	285	201	70.5%	0.48
Threshold	285	285	100.0%	0.46
Improved threshold	285	283	99.3%	0.26

[1]Differenced between retracked SSH and geoidal height

3. Gravity data for geoid determination

As stated before, our method of ocean current determination requires an accurate geoid model. To this end, we collected all possible gravity data around Taiwan. The gravity data contain surface and airborne graviyt data. The surface gravity data include land and shipborne data (Fig. 1 (a)). Land gravity data were collected over 1980-2004 by several agencies, including Academia Sinica, Base Survey Battalion and Ministry of Interior (MOI) of Taiwan. The standard errors of land gravity range from 0.04 to 1 mgal (Yen et al., 1995; Hwang et al., 2002). The shipborne gravity data were collected by international research vessels from 1960s to 1990s, and these gravity data are available at the National Geophysical Data Center (NGDC; http://www.ngdc.noaa.gov). The shipborne gravity data we used are from NGDC and have been edited by Hsu et al. (1998). The qualities of these data vary from one cruise to another. In general, measurements collected in 1990s have a better accuracy than those in the 1960s to 1980s. For example, gravity data collected by Taiwan's Ocean Researcher 1 vessel in 1996 using an Atalante KSS30 gravimeter have a mean and standard deviation of 0.3 and 2.6 mgal in the crossover differences of gravity values. According to Hsu et al. (1998), the mean and standard deviations of crossover differences of all the shipborne gravity data are 6.3 and 11.2 mgal, respectively.

The airborne gravity data were from two survey campaigns carried out from 2004 to 2008 at the heights of 5000 m and 1600 m (Fig. 1(b) and (c)). The detail of the campaign for 5000 m is given by Hwang et al. (2007). In particular, the 1600-m airborne gravity survey is to collect gravity data over the Kuroshio Current east of Taiwan, which were then used to derive a high precision, high resolution geoid model here. For both campaigns, the cross-line intervals are 4.5 km and 20 km for the north- and east-going lines, respectively. A LaCoste and Romberg System II Air-Sea gravimeter was used to collect the data. The average RMS crossover differences of gravity at intersecting lines are 2.9 mgal, and 2.7 mgal for the 5000 m and 1600 m surveys, respectively, which are equivalent to a 2-mgal point standard error. Due to signal attenuation and filtering of raw gravity data, the spatial resolution of airborne gravity data is about 6 km for the 5000-m survey, and it is shorter than 6 km for the 1600-m survey.

4. A geoid model over the Kuroshio Current and Taiwan

The method for geoid modeling is based on the remove-compute-restore (RCR) procedure. The computation of a geoidal height, *N*, is divided into three parts

$$N = N_{ref} + N_{res} + N_{rtm} \tag{5}$$

where N_{ref} is geoidal height from a geopotential model, N_{res} is the residual geoidal height and N_{rtm} is geoidal height due to the residual terrain model (RTM) (Forsberg, 1984). Accordingly, the surface (including altimeter-derived) and airborne gravity anomalies Δg^{surf} and Δg^{air} can be also spilt into three portions:

$$\Delta g^{surf} = \Delta g^{surf}_{ref} + \Delta g^{surf}_{res} + \Delta g^{surf}_{rtm} \tag{6}$$

$$\Delta g^{air} = \Delta g^{air}_{ref} + \Delta g^{air}_{res} + \Delta g^{air}_{rtm} \tag{7}$$

where Δg^{surf}_{ref} and Δg^{air}_{ref} are gravity anomalies from the same geopotential model as in Eq. (5), Δg^{air}_{res} and Δg^{surf}_{res} are residual gravity anomalies, and Δg^{surf}_{rtm} and Δg^{air}_{rtm} are RTM-derived gravity anomalies at sea level and the flight altitude. The residual geoid, N_{res}, and the error

variance were computed by

$$N_{res} = \begin{pmatrix} C_{ng^{surf}} & C_{ng^{air}} \end{pmatrix} \begin{pmatrix} C_{g^{surf}} + D_{\Delta g}^{surf} & C_{g^{surf}g^{air}} \\ C_{g^{air}g^{surf}} & C_{g^{5000}} + D_{\Delta g}^{air} \end{pmatrix}^{-1} \begin{pmatrix} \Delta g_{res}^{surf} \\ \Delta g_{res}^{air} \end{pmatrix} \quad (8)$$

$$\sigma_e = C_n - \begin{pmatrix} C_{ng^{surf}} & C_{ng^{air}} \end{pmatrix} \begin{pmatrix} C_{g^{surf}} + D_{\Delta g}^{surf} & C_{g^{surf}g^{air}} \\ C_{g^{air}g^{surf}} & C_{g^{5000}} + D_{\Delta g}^{air} \end{pmatrix}^{-1} \begin{pmatrix} C_{ng^{surf}}^T \\ C_{ng^{air}}^T \end{pmatrix} \quad (9)$$

where C_n is the variance of geoid, $C_{ng^{surf}}$ $C_{ng^{air}}$ $C_{g^{surf}}$ $C_{g^{air}g^{surf}}$ $C_{g^{air}}$ $C_{g^{surf}g^{air}}$ are covariance matrices for geoid-surface gravity anomaly, geoid-airborne gravity anomaly, surface gravity anomaly -surface gravity anomaly, airborne gravity anomaly -surface gravity anomaly, airborne gravity anomaly -airborne gravity anomaly, surface gravity anomaly -airborne gravity anomaly, and $D_{\Delta g}^{surf}$ and $D_{\Delta g}^{air}$ are the error variances of the surface and airborne gravity anomalies.

For the reference geopotential model, we adopt a combined GGM02C (Tapley et al., 2005) and EGM96 (Lemoine et al, 1998) model to degree 360. The elements of the covariance matrices in Eqs. (8) and (9) are determined from covariance functions at given spherical distances of two data points. The covariance functions are expanded into series of Legendre polynomials. For the covariance function of the disturbing potential, the coefficients of expansion are the error degree variances of the combined GGM02C-EGM06 model (for degree 2 to 360) and the model degree variances of Tscherning and Rapp (1974, Model 4, for degree 361 to infinity). Other covariance functions are derived by covariance propagation, see also Hwang and Parsons (1995). For the RTM effects, we use a $3'' \times 3''$ digital elevation model of Taiwan. Fig. 2 shows the geoid model and the error distribution. The geoid variation and the formal errors are correlated with the roughness of terrain and bathymetry. The formal errors at A, B and C are 34, 22 and 5 cm, respectively. This difference in formal error is partly due to the fact that A and B are over a rough bathymetry and C is over a smooth bathymetry, and partly due to different densities of gravity data. Note that the airborne gravity data contribute mostly to the geoidal signal at C.

It is rather difficult to carry out an external accuracy assessment of a geoid model at sea. We did an assessment on the benchmarks along coatal leveling routes shown in Fig. 2. Here the modeled and the observed geoidal heights are compared, the later being defined as the difference between the GPS-derived ellipsoidal height and the orthometric height from precision leveling. Table 2 shows the statistics of the comparison. The standard deviation of the differences in Table 2 is a descriptor of the geoid accuracy. Again, due to the smooth bathymetry and smooth gravity variation, the geoidal heights near C (north route) are better determined than those near A and B (east route). According to Table 2, we could expect a geoidal accuracy of about 5 cm near A, B and C.

Table 2: Statistics of differences (in meter) between observed and modeled geoidal heights at two leveling routes near coasts

Route	Max	Min (mgal)	Mean	Std. dev.
North	-0.035	-0.186	-0.096	0.044
East	0.160	-0.147	0.052	0.095

5. Temporal variation of ocean currents at crossovers of TOPEX and Jasons-1 ground tracks

We use altimeter data from T/P and JASON-1 and the geoid model to determine time-variation of the ocean currents east of Taiwan at two crossovers, namely A and B in Fig. 3.

These two crossovers are more than 30 km to the coasts, so the altimeter ranging will not be degraded by waveform corruption; see also Deng (2004). According to Liang et al. (2003), A and B are near the Kuroshio, where the ocean current is largely geostrophically balanced and the maximum speed may exceed 100 cms^{-1}. A is located in a zone where the Kuroshio meanders. The zonal and meridional geostrophic velocity components of ocean current at a crossover are determined by

$$u = -\frac{g}{f}\frac{\partial \varsigma}{\partial y} = -\frac{g}{f}\xi \tag{10}$$

$$v = \frac{g}{f}\frac{\partial \varsigma}{\partial x} = \frac{g}{f}\eta \tag{11}$$

where g is gravity at the crossover point, $f = 2\omega_e \sin\phi$ with ω_e being the mean rotational velocity of the earth and ϕ latitude, x and y are the zonal and meridional coordinate variables, and ξ is ocean dynamic height, defined as be determined by

$$\varsigma = h - N \tag{12}$$

where h is sea surface height from satellite altimetry and N is geoidal height. At the crossover of two satellite ground tracks, the gradients of DOT along the ascending and descending tracks, ε_a and ε_d, can be expressed by the east and north gradient components as (Hwang and Chen, 2000)

$$\xi = \frac{\varepsilon_a \cos\alpha_d - \varepsilon_d \cos\alpha_a}{\sin(\alpha_a - \alpha_d)} \tag{13}$$

$$\eta = \frac{-\varepsilon_a \sin\alpha_d + \varepsilon_d \sin\alpha_a}{\sin(\alpha_a - \alpha_d)} \tag{14}$$

Figs. 4 and 5 show the time series of ocean current velocities at A, B at filter widths of 40, 80 and 120 km. Due to missing satellite passes and/or missing height observables near the crossovers, these time series all contain gaps. The altimeter-derived velocities were then compared with in-situ velocities computed from drifter data (Fig. 6). The drifter data are from the World Ocean Circulation Experiment (WOCE) database (http://woce.nodc.noaa.gov/wdiu/). A drifter-derived velocity was computed as the ratio of traveling distance and the difference of times between two successive records. Because a drifter is not likely to exactly pass through any of the crossovers, we use drifter data within a 0.1° box centered at the crossover. The altimeter-derived velocities were also compared with the model-derived velocities of Wu and Hsin (2005). The model of Wu and Hsin (2005), driven by winds and sea surface temperature, is based on the Princeton Ocean Model (POM; Blumberg and Mellor, 1987) and the boundary conditions of East Asia Marginal Seas (EAMS). Below is a summary and discussion based on the

results in Figs. 6 to 8.

1) Crossover A

At a filter width< 120 km, the altimeter-derived velocities are larger than the model and drifter-derived velocities, and the directions of flows from three results are reasonably consistent. At filter width= 120 km, the magnitudes of velocities from all results differ by about 10 cms^{-1}. At any filter width, the directions of flows from all results are mostly northward or northeastward. In rare cases the altimeter and model-derived currents turn southwards. The drifter-derived currents are nearly northward in most cases. Since the Kuroshio meanders around A, the ocean currents here fluctuate rapidly. This fluctuation is also seen in Fig. 4.

2) Crossover B

Here in most cases the altimeter-derived velocities exceed 200 cms^{-1} and are larger than the drifter and model-derived velocities at any filter width. In some cases, the drifter-derived velocities are nearly 200 cms^{-1}, otherwise fall between the altimeter and model-derived velocities. Compared to A, the velocities at B from the altimetry and the POM model appear to be more time independent, and the directions of flows are uniform throughout the entire year. Note that the altimeter-derived velocities (filter width= 120 km) at A and B agree well with the velocities given in Liang et al. (2003).

3) Interannual variation

In order to see the temporally filtered velocities and in particular the interannual variation, we applied the same Gaussian filter to these time series using a filter width of 12 months for the 120-km filtered time series. The results are given in Fig. 7. The time-filtered, altimeter-derived velocities seem to be rather smooth at all crossovers. At A, the pattern of velocity did not repeat exactly from one year to another, and the ocean currents in 2005 were the weakest. At B, the ocean currents are quite stable interannually. A possible explanation for this stability is that, B is almost at the axis of the Kuroshio, which maintains a steady flow from one year to another.

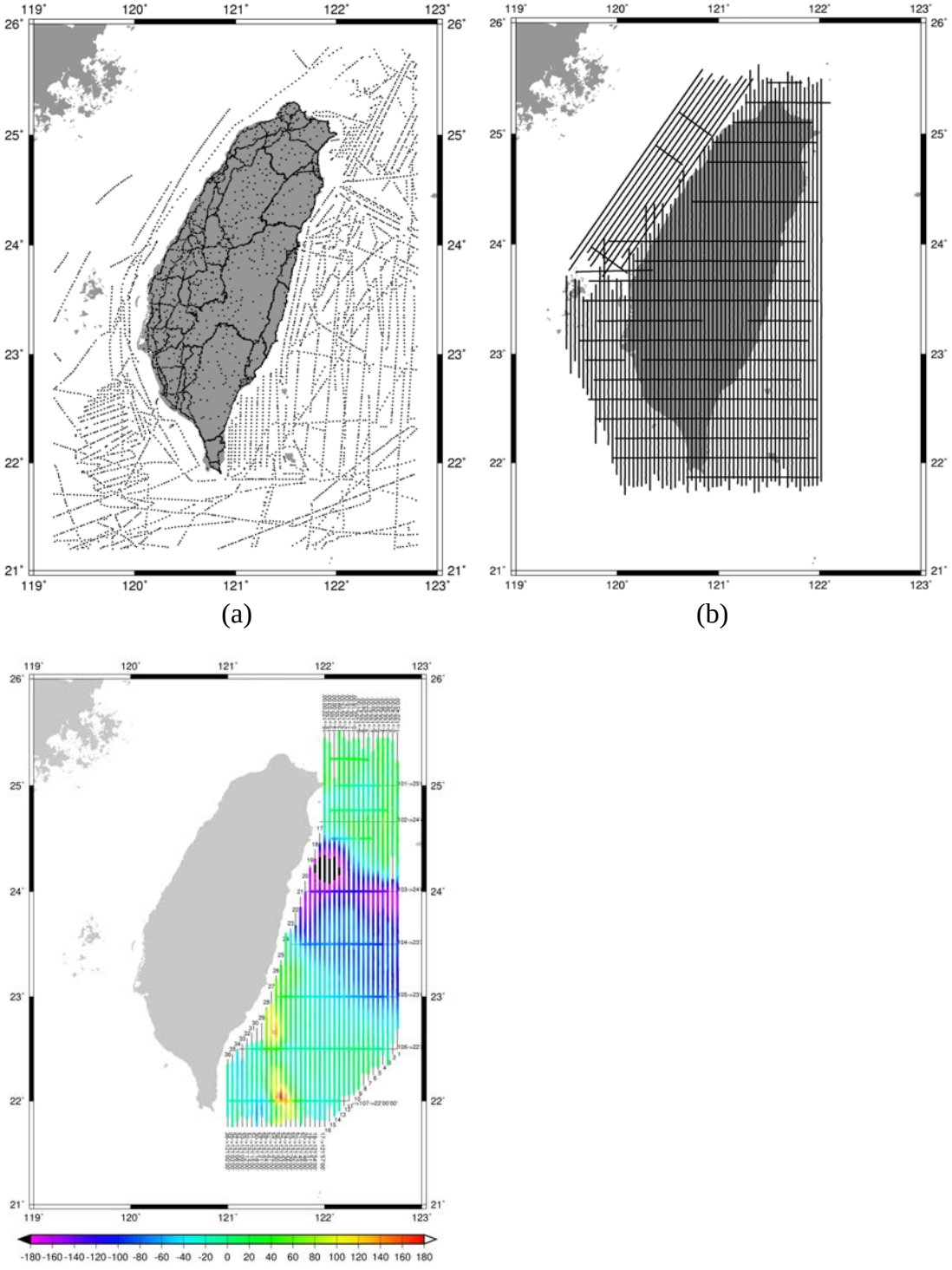

Fig. 1: Distributions of (a) land and shipborne gravity data (b) airborne gravity data at 5000 m (c) airborne gravity data at 1600 m

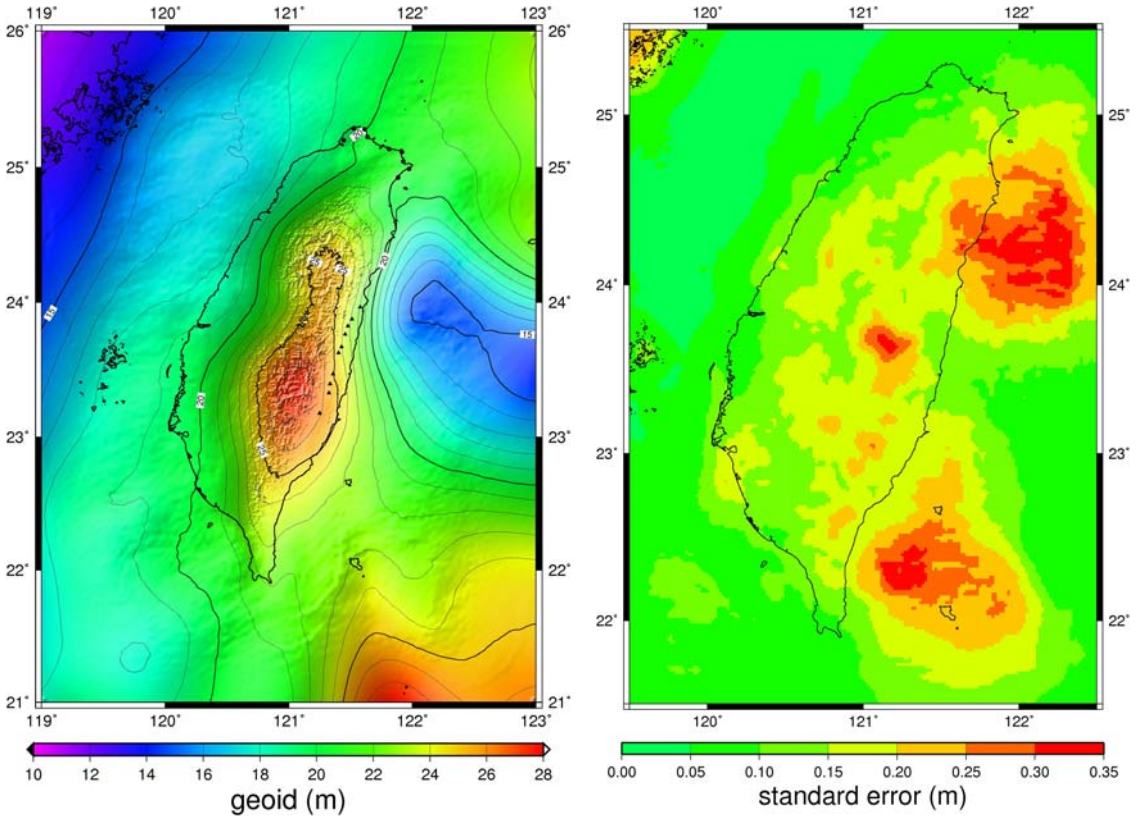

Fig. 2: Geoid undulations and standard errors. The circles (left panel) represent the leveling benchmarks for geoid model evaluation (Table 2).

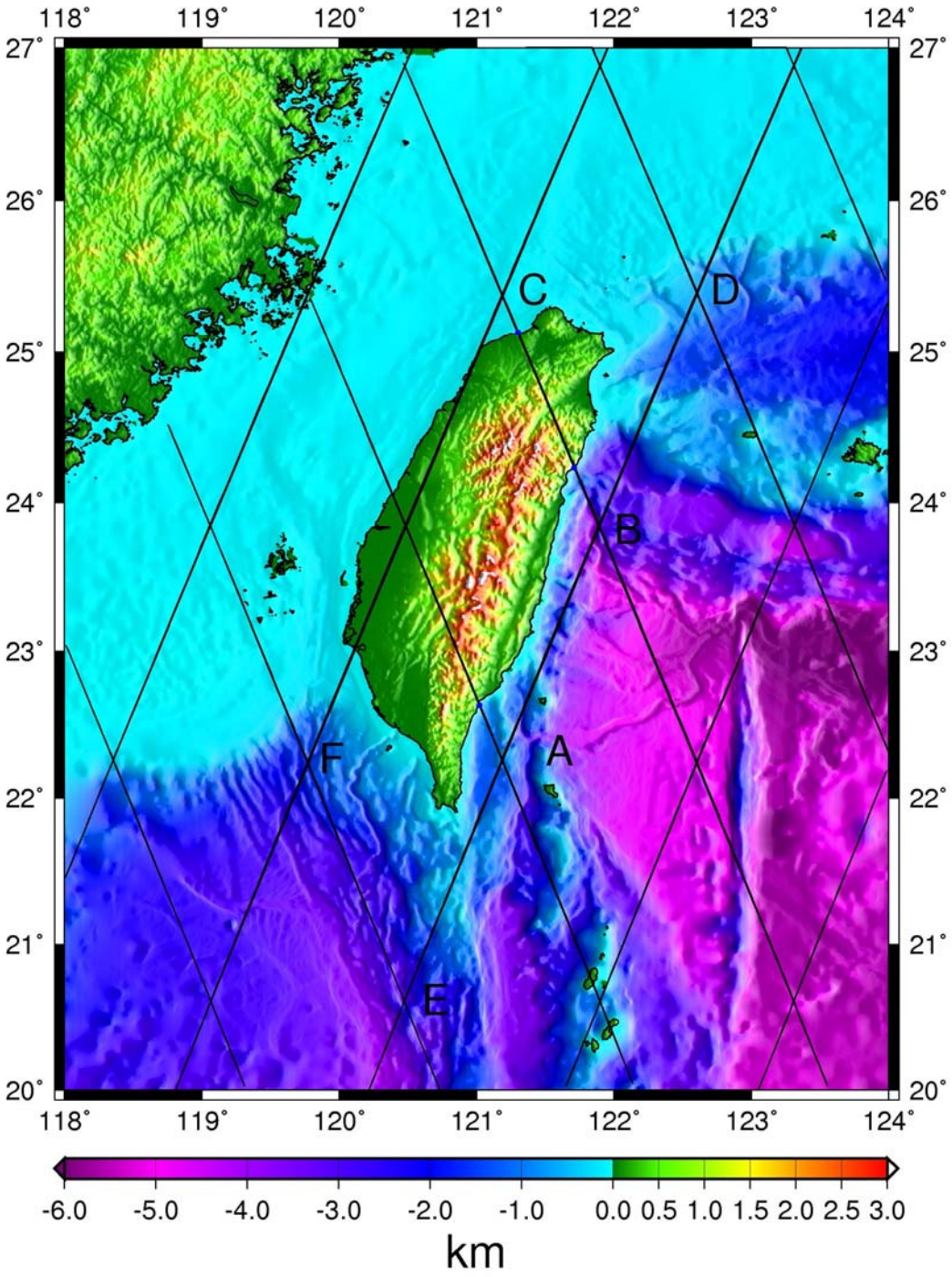

Fig. 3: Distribution of T/P and JASON-1 crossovers around Taiwan.

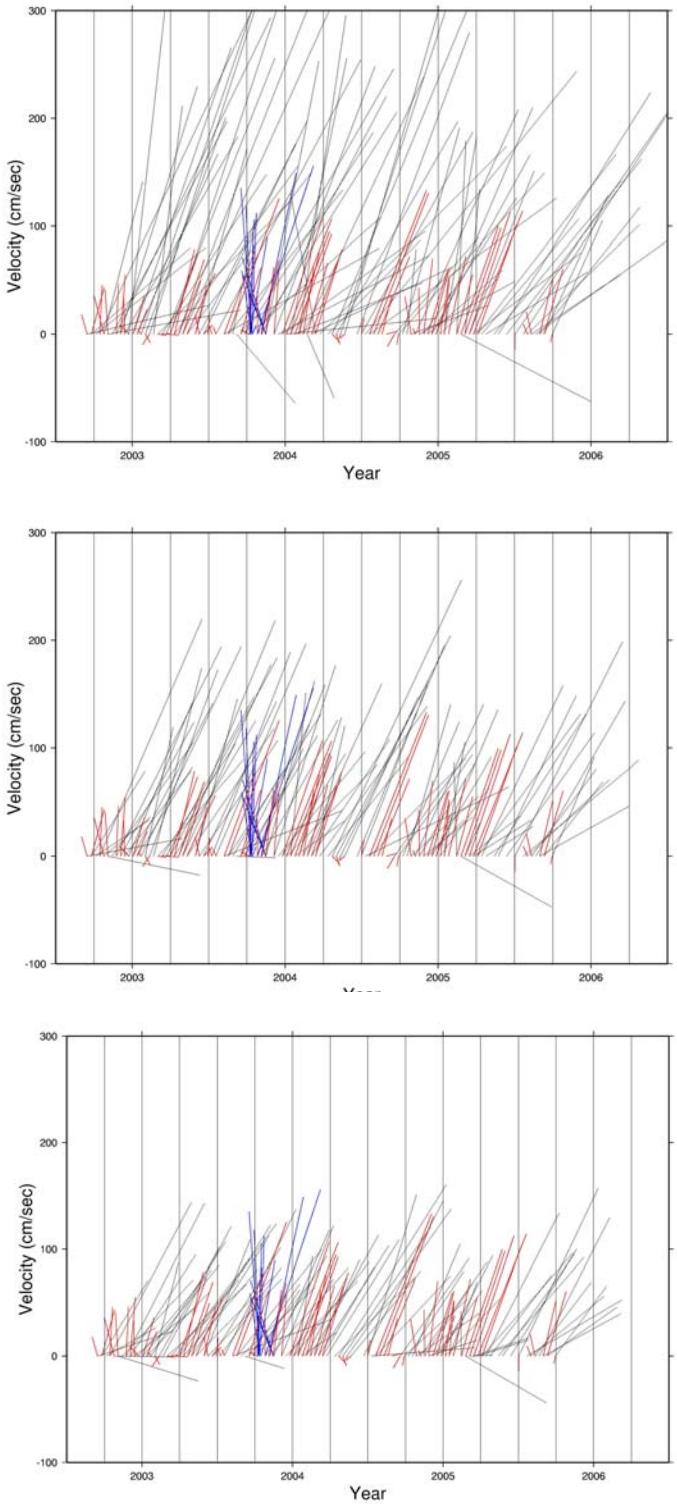

Fig. 4: Ocean current velocity at crossover A from altimetry (black), model (red) and drifter (blue). Filter widths of 40 (top), 80, 100 (bottom) km are used in the altimeter-derived velocities.

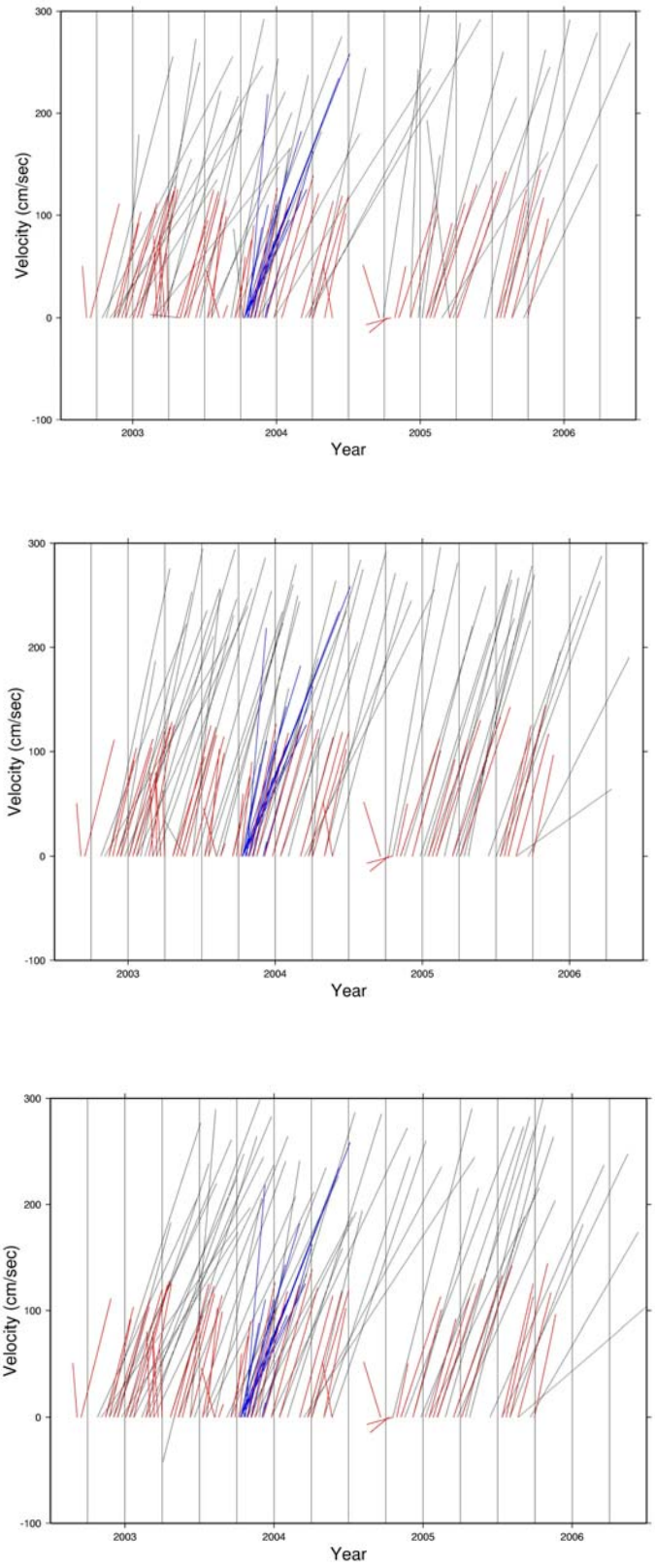

Fig. 5: Same as Fig. 4, but for crossover B

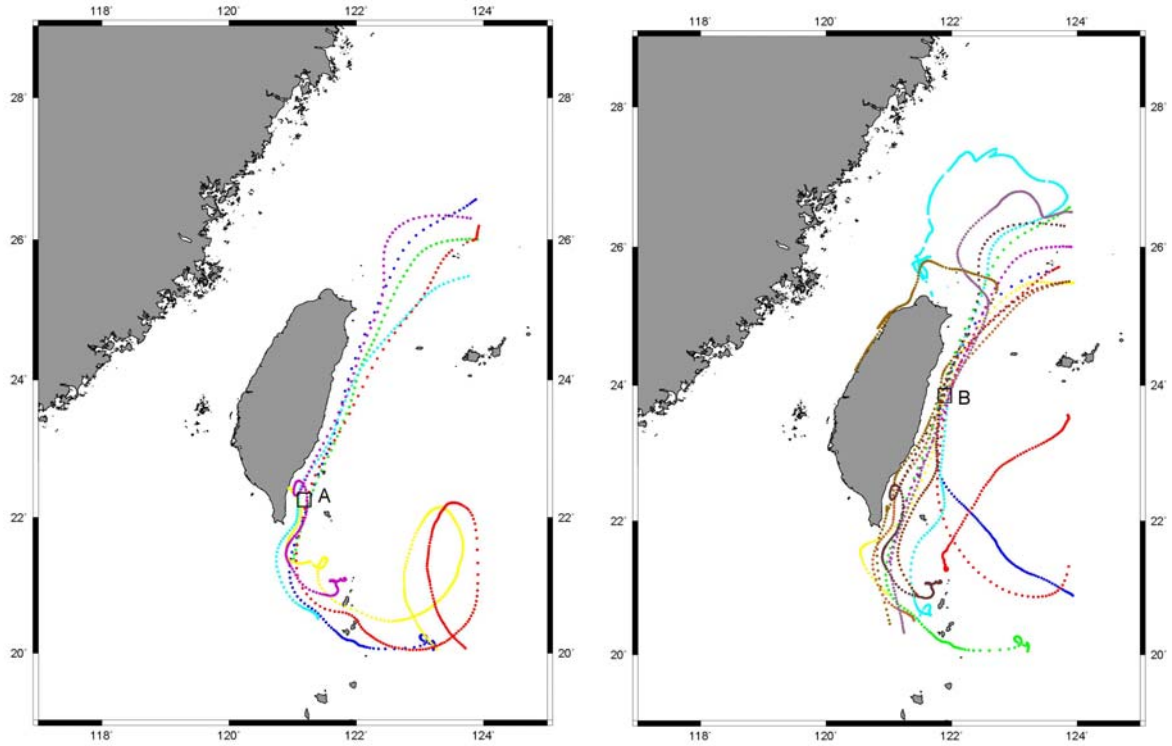

Fig. 6: Tracks of drifters. The drifter data in the boxes are used for comparison with altimeter-derived velocities.

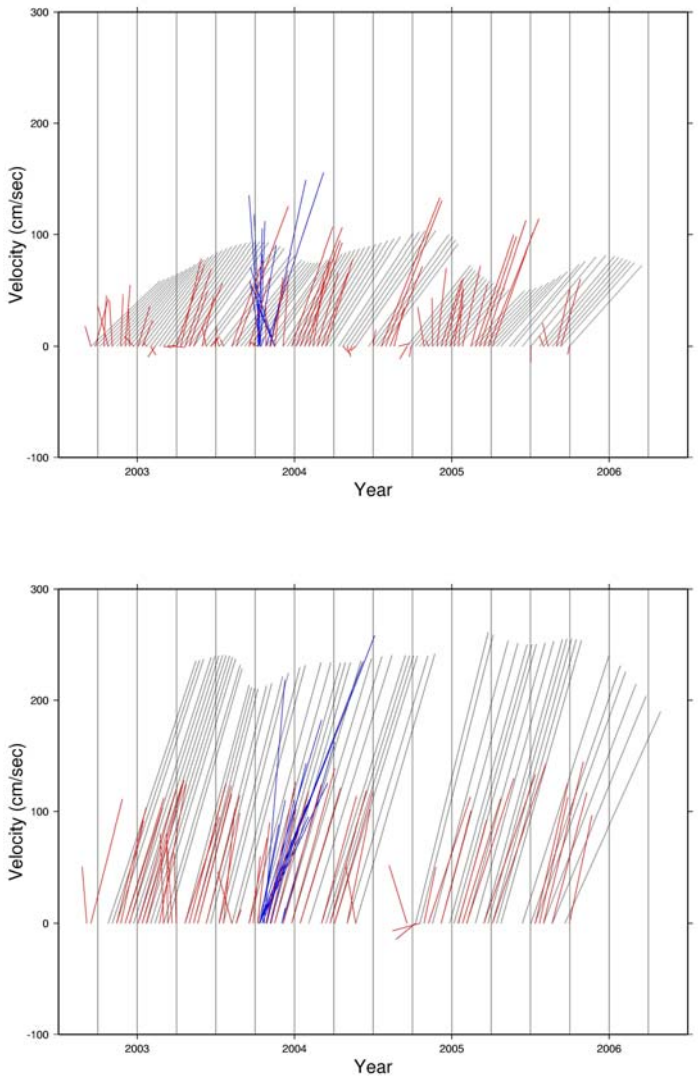

Fig. 7: Interannual variation of velocity at A (top) and B. The legend is the same as that in Fig. 4.

6. Conclusions

In this project, we develop a detailed geoid model over the Kuroshio Current east of Taiwan, which is used to study the temporal variation of the Kuroshio Current at two crossovers. The geoid model obtained in this project can also be used to compute a two-dimensional geostrophic velocity field around Taiwan. That is, the geoid can be used to compute a grid of DOT using altimeter data from multi-missions such as T/P, JASON-1, ERS and ENVISAT. Even data from the laser altimeter mission ICESat (Schutz et al., 2005) can be used to enhance data coverage, especially around coasts. Again, given the current DOT accuracy, the spatial resolution of a 2-D velocity field will be at the mesoscale level (coarser than 100 km). Since the condition of geostrophic balance does not strictly hold over shallow waters (e.g., the Taiwan Strait), a better approach of obtaining ocean current velocities here is to assimilate altimeter data into such ocean dynamic model as POM; see also the discussion in Le Provost and Bremond (2003).

Reasonably good ocean currents at a spatial scale larger than 100 km were obtained from

T/P and JASON-1 altimetry at crossovers A and B (the Kuroshio area), 7). It is possible to improve our results at A and B by taking into account the following points.

1) The marine gravity data must be improved in both coverage and accuracy. The systematic and random errors associated with the marine gravity data used in this paper must be further calibrated.

2) The current technique of geoid modeling is optimal for land, but might not be so for the sea. An improved marine geoid around Taiwan is needed

3) An improved tide model over the Taiwan Strait is needed. This can be achieved by assimilating tidal constants at tide gauges and altimeter SSHs into a hydrodynamic model with a fine-resolution bathymetry model.

7. Publications related to this project (2005-2008)

Published SCI journal papers:

Hwang, C., J. Guo, X. Deng, H.Y. Hsu and Y. Liu, Coastal gravity anomaly from retracked Geosat/GM altimetry: improvement, limitation and the role of airborne gravity data, DOI10.1007/s00190-062-0052-x, Journal of Geodesy, 2006. (IF=1.210)

Guo, JY, C Hwang, XT Chang, and YT Liu, Improved threshold retracker for satellite altimeter waveform retracking over coastal sea, Progress in Natural Science, 16 (7), pp. 732-738, 2006. (IF=0.531)

Chang, XT JC Li , JY Guo JY, and C Hwang , A multi-leading edge and multi-threshold waveform retracker, Chinese Journal Of Geophysics-Chinese Edition 49 (6), pp. 1629-1634, 2006. (IF =0.559)

Hwang, C., Y.S. Hsiao, H.C. Shih, M. Yang, K.H. Chen, R. Forsberg and A. V. Olesen, Geodetic and geophysical results from a Taiwan airborne gravity survey: Data reduction and accuracy assessment, Journal of Geophysical Research, 112, DOI:10.1029/2005JB004220, 2007. (IF=2.800)

Hwang, C, and HY Hsu, Shallow-water gravity anomalies from satellite altimetry: case studies in the East China Sea and Taiwan Strait, Journal of the Chinese Institute of Engineers, Vol. 31, No. 5, pp. 841-851, 2008. (IF =0.190)

Hwang, C, J Benveniste, Y Dang, and C. K. Shum, Preface to the Special Issue on satellite Altimetry over Land and Coastal Zones: Applications and Challenges, Vol. 19, No. 1-2, I. DOI:10.3319/TAO.2008.19.1-2.0(SA) (IF=0.835)

Hwang, C, HC Shih, JY Guo, and YS Hsiao, Zonal and meridional ocean currents at TOPEX/Poseidon and JASON-1 crossovers around Taiwan: error analysis and limitation, Terrestrial, Atmospheric and Oceanic Sciences (TAO), Vol. 19, No.1-2, pp. 151-162,2008. DOI:10.3319/TAO.2008.19.1-2.151(SA) (IF=0.856)

References

Anzenhofer, M., C. K. Shum, and M. Renstch, 2002: Coastal Altimetry and Applications, The Ohio State University, Columbus, USA, 36 pp.

Brown, G.S., 1977: The average impulse response of a rough surface and its applications. IEEE Trans Ant Prop AP-25 (1): 67-74

Blumberg, A. F., and G. L. Mellor, 1987: A description of a three-dimensional coastal ocean circulation model. In: Heaps, N.S. (ed.), Coastal and Estuarine Sciences 4: three dimensional coastal model, AGU, Washington, D.C., 1-16.

Chang, XT JC Li , JY Guo JY, and C Hwang , A multi-leading edge and multi-threshold waveform retracker, Chinese Journal Of Geophysics-Chinese Edition 49 (6), pp. 1629-1634, 2006.

Chen, C. T. A., and D. D. Shen, 2006: Does the Taiwan Warm Current originate in the Taiwan Strait in wintertime? J. Geophys. Res-Oceans., **111**, Art. No. C04005.

Deng, X, 2004: Improvement of geodetic parameter estimation in coastal regions from satellite radar altimetry. PhD thesis, Curtin University, Australia.

Forsberg, R, 1984: A study of terrain reductions, density anomalies and geophysical inversion methods in Gravity Field modeling. Reports of department of geodetic Science and Surveying, No 355, The Ohio State University, Columbus, Ohio.

Fu, L. L., E. J. Christensen, C. A. Yamarone, Jr. M. Lefebvre, Y. Menard, M. Dorrer, and P. Escudier, 1994: TOPEX/Poseidon mission overview. J. Geophys. Res., **99**, 24369-24382.

Fu, L. L, and A. Cazenave, 2001: Satellite Altimetry and Earth Sciences, Academic Press, San Diego.

Guo, J.Y., C. Hwang, X.T. Chang, and Y.T. Liu, 2006: Improved threshold retracker for satellite altimeter waveform retracking over coastal sea, Progress in Natural Science, 16 (7), pp. 732-738,.

Hsu, S. K., C. S. Liu, C. T. Shyu, S. Y. Liu, J. C. Sibuet, S. Lallemand, C. Wang, and D. Reed, 1998: New Gravity and Magnetic Anomaly Maps in the Taiwan-Luzon Region and their Preliminary Interpretation. Terr. Atmos. Oceanic., **9**, 509-532.

Hwang, C., and B. Parsons, 1995: Gravity anomalies derived from Seasat, Geosat, ERS-1 and Topex/Poseidon altimeter and ship gravity: a case study over the Reykjanes Ridge, Geophys. J. Int., **122**, 551-568.

Hwang, C., and S. A. Chen, 2000: Circulations and eddies over the South China Sea derived from TOPEX/POSEIDON altimeter data. J. Geophys. Res., **105**, 23943-23965.

Hwang, C., and R. Kao, 2002: TOPEX/POSEIDON-derived space-time variations of Kuroshio Current: applications of a gravimetric geoid and wavelet analysis. Geophys. J. Int., **151**, 835-847.

Hwang, C., and B. Parsons, 1995: Gravity anomalies derived from Seasat, Geosat, ERS-1 and Topex/Poseidon altimeter and ship gravity: a case study over the Reykjanes Ridge, Geophys. J. Int., **122**, 551-568.

Hwang, C., C. R. Wu, and R. Kao, 2004: TOPEX//Poseidon observations of mesoscale eddies over the Subtropical Countercurrent: Kinematic characteristics of an anticyclonic eddy and a cyclonic eddy. J. Geophys. Res., **109**, C08013, doi:10.1029/2003JC002026.

Hwang, C., J. Guo, X. Deng, H.Y. Hsu and Y. Liu, Coastal gravity anomaly from retracked Geosat/GM altimetry: improvement, limitation and the role of airborne gravity data, DOI10.1007/s00190-062-0052-x, Journal of Geodesy, 2006.

Hwang, C., Y.S. Hsiao, H.C. Shih, M. Yang, K.H. Chen, R. Forsberg and A. V. Olesen, Geodetic and geophysical results from a Taiwan airborne gravity survey: Data reduction and

accuracy assessment, Journal of Geophysical Research, 112, DOI:10.1029/2005JB004220, 2007.

Hwang, C., and H.Y. Hsu, 2008: Shallow-water gravity anomalies from satellite altimetry: case studies in the East China Sea and Taiwan Strait, Journal of the Chinese Institute of Engineers, Vol. 31, No. 5, pp. 841-851.

Lemoine, F. G., S. C. Kenyon, J. K. Factor, R. G. Trimmer, N. K. Pavlis, D. S. Chinn, C. M. Cox, S. M. Klosko, S. B. Luthcke, M. H. Torrence, Y. M. Wang, R. G. Williamson, E. C. Pavlis, R. H. Rapp, and T. R. Olson, 1998: The development of joint NASA GSFC and the National Imagery and Mapping Agency (NIMA) Geopotential Model EGM96. Rep. NASA/TP-1998-20686, 575pp., National Aeronautics and Space Administration, Greenbelt, MD.

Le Provost, C., and M. Bremond, 2003: Resolution needed for an adequate determination of the mean ocean circulation from altimetry and an improved geoid. Space Sci. Rev., **108**, 163-178.

Liang, W. D., T. Y. Tang, Y. J. Yang, M. T. Ko, and W. S. Chuang, 2003: Upper-ocean currents around Taiwan. Deep-Sea Res. Pt. II., **50**, 1085-1105.

Martin TV, Zwally HJ, Brenner AC, Bindschadler RA (1983) Analysis and Retracking of continental ice sheet radar altimeter waveforms. J Geophys Res 88: 1608-1616

Tang, T. Y., J. H. Tai, and Y. J. Yang, 2000: The flow pattern north of Taiwan and the migration of the Kuroshio. Cont. Shelf. Res., **20**, 349-371.

Tapley, B., J. Ries, S. Bettadpur, D. Chambers, M. Cheng, F. Condi, B. Gunter, Z. Kang, P.Nagel, R. Pastor, T. Pekker, S.Poole, F. Wang, 2005: GGM02 - An improved Earth gravity field model from GRACE, J. Geod, 79, 467-478.

Tscherning, C. C., and R. H. Rapp, 1974: Closed covariance expressions for gravity anomalies, geoid undulations and deflections of the vertical implied by anomaly Degree variance models. Reports of department of geodetic Science and Surveying, No 208, The Ohio State University, Columbus, Ohio.

Wessel, P., and W. H. F. Smith, 1999: The Generic Mapping Tools (GMT). Technical Reference and Cookbook, Univ. of Hawaii, USA.

Wu, C. R and Y. C. Hsin, 2005: Volume transport through the Taiwan Strait: A numerical study. Terr. Atmos. Oceanic., **16**, 377-391

Yen, H. Y., Y. H. Yeh, C. H. Lin, K. J. Chen, and Y. B. Tsai, 1995: Gravity survey of Taiwan. J Phys Earth, **43**, 685-696.

Zhang, D., T. N. Lee, and W. E. Johns, 2001: The Kuroshio east of Taiwan: modes of variability and relationship to interior ocean mesoscale eddies. J. Phys. Oceanogr., **31**, 1054-1074.